Estimating the section elevation angle of cubes on a cubic mesh. Application to nickel microstructure size estimation.

Christian Germain, Rémi Blanc, Marc Donias, Olivier Lavialle, Jean-Pierre da Costa, Pierre Baylou

GERMAIN C ET AL: ESTIMATING THE SECTION ELEVATION ANGLE OF CUBES ON A CUBIC MESH. APPLICATION TO NICKEL MICROSTRUCTURE SIZE ESTIMATION.

Abbreviated Title
ESTIMATING THE SECTION ANGLE OF CUBES ON A CUBIC MESH FOR NICKEL SUPERALLOY CHARACTERISATION.

Christian GERMAIN, Rémy BLANC, Marc DONIAS, Olivier. LAVIALLE, Jean-Pierre DA COSTA, Pierre BAYLOU
christian.germain@laps.u-bordeaux1.fr, remy.blanc@laps.u-bordeaux1.fr , donias@enseirb.fr, jean-pierre.dacosta@laps.u-bordeaux1.fr, olivier.lavialle@laps.u-bordeaux1.fr
Equipe Signal et Image, LAPS - UMR 5131 CNRS – ENSEIRB, ENITAB,
Bordeaux1 University, 351 cours de la Libération - 33405 Talence cedex - France

Abstract
The paper discusses two new image analysis methods for the estimation of the elevation angle of the section plane of a material. These methods are applicable to materials such as nickel base superalloys, the microstructure of which shows cubes arranged on a cubic regular grid. 3-D models were proposed which help interpreting the section images and validating our approach. Our first method operates in the Fourier domain, and is based on the estimation of the spatial frequencies of the network of lines observed on the section. The second method is based on the average distance measured between hazy areas. Both methods are independent. Applied to synthetic images or to real material samples, they produce comparable estimations. The values of the elevation angle allow us to cancel the bias associated with the estimation of the material pattern dimensions.
Keywords: cubic mesh, elevation angle, nickel superalloy, size estimation, 3-D simulation

I. INTRODUCTION

Microstructure of monocrystalline nickel base superalloys consists of two phases called γ and γ’. The γ’ phase appears as a rectangular grid of quasi parallelepipedal particles. The mean size of a particle side is about 400 nanometres. The γ phase constitutes walls and provides with a partition between the γ’ nodules. The thickness of the γ walls is roughly ten nanometres.

An appropriate specimen etching causes some altitude differences between the two phases. The scanning electron microscope transforms the altitude differences into grey scale variations.

Fig 1 On Fig. 1a, γ’ sections appear in dark grey and they are most frequently shaped as parallelograms. The intersections of γ walls appear in light grey. Some irregular and intermediate grey shapes also appear. They are called hazy areas. They are usually considered as phases with intermediate chemical properties. We will propose an interpretation for these hazy areas in section II.

Estimating the size of γ’ particles is necessary in order to control the physical and mechanical properties of the nickel base superalloy. One approach for such an estimation consists in characterising the material using a morphological analysis of γ’ particles (Georget *et al.*, 1990). More specifically, this approach is based on the statistical measurement of the sizes of the parallelepiped sides and on the estimation of the average side size supposed to be identical along each of the three main crystal axes.

Unfortunately, these measurements are affected by the elevation angle between the sectioning plane and the main directions of the crystal. Indeed, a non-zero elevation angle leads to the

overestimation of the parallelepiped sizes whereas an oblique section plane has no effect on the relationship between surface and volume ratios (Russ *et al.*, 2000) (Blanc *et al.*, 2004).
In this paper, we address the correction of the influence of the section plane elevation angle on the stereological size estimation of a set of cubes arranged on a cubic mesh. For such a purpose, we propose two methods, each allowing the estimation of the azimuth φ and the elevation angle θ of the section plane. Both angles correspond to the 3-D reference system associated with the main directions of the crystal as described in Fig. 1b.
In section II.1, we will propose a 3-D model of the material and provide with 3-D simulations of section images. Within the context of these simulations, we will present the effect of the inclination of the section plane on the image aspect. It will allow us to propose an interpretation for the hazy areas observed on real images.
In section II.2, we will propose a first method for the estimation of the elevation angle θ from the transformation of the section image in the Fourier domain. Indeed, in this space, the mean orientations of the sides of γ' modules are detectable.
In section II.3 we will introduce a competing approach for elevation angle θ estimation. This approach is based on the analysis of the hazy areas.
In section III, we will provide some results obtained with SEM images of nickel base superalloy using both estimation approaches. We will also specify the correction to apply to the morphological measurements of *γ'* particles and will discuss the results obtained.
Finally, section IV will be devoted to the conclusion.

II. MATERIAL AND METHOD

II.1 Three-dimensional model and simulations

In this section we introduce a 3-D model which describes the morphology of the phases γ and γ' which compose a mono-crystal nickel base superalloy. This model allows to simulate the γ/γ' intersection with a sloped plane. In a first stage, our model uses identical cubes arranged on a regular cubic mesh. The length of the cube side is given by the constant value *c* and the width of the separation wall is the constant value *e* (Fig. 2 a).
For such a material, a horizontal section, parallel to one of the principal directions of the cube,
Fig. 2 could produce either an image showing squares disposed on a regular grid (Fig. 2b , section plane A) or a uniformly white picture (section plane B) .
Fig. 3 When the section plane parameters are φ=0° and $\theta \neq 0°$ (Fig. 3), the intersection shows rectangles.
Some rectangle sides are related to the size of the cubes (*c* and $c/\cos\theta$), while some other rectangles have one side related to the size of the cube *c* and the other side related to the vertical position of the section plane. Only the rectangles of the first kind allow the reconstruction of the morphological parameters of the material.
Fig. 4a shows the various intersections observed on a vertical view. Fig. 4b shows the image
Fig. 4 of the corresponding section plane.
In order to qualify our model, we have simulated some images of section planes with various azimuth and elevation angles. Figure 5a shows such a simulation with φ=0° and θ=20°. We observe that this image is in accordance with the prediction given on Fig. 4b.
Fig. 5 On Fig. 5b we have carried out another simulation with φ=45° and θ=20°. Using this azimuth, we can notice that the complete intersections of cubic particles are diamond shaped whereas incomplete intersections show triangular and pentagonal shapes.
In order to obtain more realistic simulations, we have also introduced fluctuations in the previous model. We have replaced the cubes by parallelepipeds and slightly shifted their locations. The model becomes irregular and thus provides with a better description of the real material layout.

Fig. 6 Fig. 6a shows the simulation of a section drawn according to this new model. The section plane crosses several γ layers, thus forming several large γ areas surrounded by γ' squares. Theses areas give an interpretation for the hazy areas observed on the real sections. Indeed, both kinds of areas have consistent shapes. Moreover, the grey scale variations inside the hazy areas can be explained by the chemical etching of the γ phase. Results in section III will confirm this interpretation for various azimuth and elevation angles. Fig. 6b confirms that our model is realistic when $\varphi \neq 0°$ and $\theta \neq 0°$.

Let us note that the implementation of our models have been programmed in C language using a Microsoft Windows station.

II.2 Estimation of the elevation angle in the Fourier domain.

The complete intersection between a cube and an oblique section plane is a parallelogram. In our case, the set of cubes forms two networks of equidistant parallel lines on the section plane. Let d_1 be the period of one network, d_2 the period of the second one, and ω the angle between the two networks. d_1 and d_2 are related to the parallelogram shape of the γ' particle

Fig. 7 (Fig. 7).

We can deduce the azimuth φ and the elevation angle θ from d_1, d_2 and ω.

$$\varphi = Arc\tan\sqrt{\frac{1-r^2+\sqrt{\Delta}}{r^2-1+\sqrt{\Delta}}} \text{ and } \theta = Arc\tan\sqrt{\frac{2\sqrt{\Delta}}{1+r^2-\sqrt{\Delta}}} \quad (1)$$

$$\text{with } \Delta = r^4 + \left(4\cos^2\omega - 2\right) r^2 + 1 \text{ and } r = d_1 / d_2 \quad (2)$$

The estimation of d_1 and d_2 is much easier in the Fourier domain, considering the periodicity of networks. Actually, the 2-D Fourier transform F(i,j) computed from the grey levels f(x,y)

Fig. 8 of an image represent the luminance changes with respect to spatial distances (Jain, 1989). Thus, when a peak appears in the Fourier spectrum, the coordinates (i,j) of this peak allow to obtain directly the frequency and the orientation of the corresponding periodic pattern appearing in the image.

The Fig. 8b shows the central area of the Fourier spectrum of the image in Fig. 8a. The contrast has been enhanced, in order to improve the visibility. Indeed, two significant pairs of peaks appear on this spectrum around the central blob. They correspond to the frequencies $f_1=1/d_1$ and $f_2=1/d_2$. Knowing f_1 and f_2 allows us to compute d_1 and d_2 and then θ and φ, according to Eq.1. The angle ω between the two networks can be measured using either the image or the Fourier spectrum according to the quality of the Fourier spectrum.

II.3 Estimation of the section plane elevation angle using the hazy areas

As shown in section II.1, the intersection between the section plane and the various horizontal γ layers produces some hazy areas.

Let c be the size of γ' cubes, e the width of γ walls, and D the distance between two consecutive hazy areas, then $(c+e)/D=\sin(\theta)$ and finally:

$$\theta = Arc\sin\left(\frac{c+e}{D}\right) \quad (3)$$

Considering the width e as a fraction of the size c, $c+e=k.c$, we obtain:

$$\theta = Arc\sin\left(\frac{c+e}{D}\right) = Arc\sin\left(\frac{k.c}{D}\right) \qquad (4)$$

Fig. 9 The average value of D can be measured on the image. Indeed, on Fig. 8a we can observe quasi parallel hazy areas. The main difficulty lies in the estimation of c. The value of c is estimated using the average S of the surface of the complete intersections between the section plane and the γ'particle.

$$S = \frac{c^2}{\cos\theta} \qquad (5)$$

Using Eq. 4 and Eq. 5 we obtain the expression of θ:

$$\theta = Arc\cos\left(\frac{\pm\sqrt{k^4S^2 + 4D^4} - k^2S}{2D^2}\right) \qquad (6)$$

Let us note that when the size c is far larger than the width e, k become close to 1. Thus, we can obtain an approximate expression for Eq. 3, which does not involve the measurement of the ratio between c and e.

$$\theta = Arc\sin\left(\frac{c+e}{D}\right) \cong Arc\sin\left(\frac{c}{D}\right) \qquad (7)$$

Eq. 6 then becomes:

$$\theta = Arc\cos\left(\frac{\pm\sqrt{S^2 + 4D^4} - S}{2D^2}\right) \qquad (8)$$

Nevertheless, if the width e is not insignificant, this expression will underestimate θ.

III. RESULTS

In order to assess the accuracy of both methods, experiments using sections taken from synthetic 3-D blocks were carried out. The 3-D blocks used are based on our most realistic model, introduced in section II.1. The elevation angle θ of the sections goes from 0° to 35°, with φ=25°. We used Eq. 1 for the estimation of θ based on the Fourier spectrum and Eq. 6 for the method based on the hazy areas.

For both methods, size, surface, angle and frequency measurements have been computed on a Microsoft Windows PC using the Aphelion software version 3.2g.

The results obtained for theses synthetic images are presented in Fig. 10. It shows that the method based on the hazy areas gives very accurate estimation of the elevation angle, since
Fig. 10 the largest deviation is less than 0.2°. The method based on Fourier spectrum is more sensitive to the accuracy of the location of the peak. Nevertheless, the deviation observed is always less than 2°. This angular deviation is equivalent to 0.7% deviation for the correction factor.

Experiments using real nickel superalloy sections have also been carried out. Theses sections show various azimuth and elevation angles and are shown in Fig. 11.

Fig. 11 The estimations of the elevation angle using both approaches are given in Table 1.

The results provided by both approaches are consistent since the differences observed
Table 1 between the Fourier spectrum and the hazy area methods are always less than 4.2°.
Besides, in case of images coming from the same material section, i.e. Fig; 11e and Fig. 11f, the elevation angle estimates given by each method are closer than 1°.

The differences observed between the two approaches come from the lack of periodicity within the material. Therefore, it becomes more difficult to estimate the average value of k, S and D in Eq. 6 and especially, and of $d1$ and $d2$ in Eq.1 and Eq.2.
Regarding the Fourier domain approach, one origin of the estimation uncertainty is the following fact. If the modes of the spectrum indicate the most likely frequencies, the inverses of theses frequencies are not necessarily the most probable periods. The exact computation of these periods requires the knowledge of the measurement scattering. Moreover, the noise affecting the sections and the size variation of γ' particles make difficult to locate accurately the peaks in the Fourier Spectrum.
In the case of the hazy areas approach, the accuracy of the estimation of θ relies on the estimations of S and D. The accuracy of S depends on the good selection of complete intersections. Besides, the undulation of the γ layers reduces the estimation accuracy of the distance D on the image.
Nevertheless, averaging the results given by both approaches allows to provide the correction factor $f=(\cos\theta)^{1/2}$ for the average size c of the γ' particles, thus cancelling the overestimation bias (Table 2). The worst bias factor observed in our image database is $f=+10.2\%$ with $\theta=36.2°$ for the section in fig. 11.a.

Table 2

Let us note that we did not compute any estimation of the elevation on the section shown in Fig. 11i, since no periodicity appears between hazy areas. It means that either the periodicity does not exist, or this periodicity is greater than the size of the image. In both cases, the elevation angle is less than 5°, and the overestimation of the particle size is smaller than 0.1% and does not need to be corrected.

IV. CONCLUSION

In this paper, we have introduced two new methods for the estimation of the elevation angle of the section plane. These methods can be applied on materials such as nickel base superalloys, which microstructure shows cubes arranged on a cubic regular grid.
In order to validate our approaches and to help the interpretation of the section images, we also introduced 3-D models for this kind of materials. From these models, we have drawn simulations of section images which appear to be realistic compared to real section images. Both methods, exercised on synthetic images drawn from our 3-D model, provide very accurate estimations of the elevation angle. When applied to real material samples, they give independent and comparable estimations.
The resulting values of the elevation angle of the section plane allow us to improve the characterisation of the microstructure, thus cancelling the bias for the estimation of the particle size, which can exceed 10% in the worst cases.
Since both methods are complementary, we are currently working on the combination of their results, in order to improve the accuracy of our elevation angle estimation.

ACKNOWLEDGEMENTS
This work has been partly funded by the Region Aquitaine, with the financial and technical support of the Safran group.

REFERENCES

Blanc R, Germain Ch, Da Costa JP, Baylou P, Cataldi C (2005). Fiber orientation measurements in composite materials. To be published in the Journal of Composite Material. Part A.
Georget D, Peyroutou P (1990). Characterization of the γ' phase in a superalloy by image analysis, In: Proceedings of the High Temperature Materials for Power Engineering Conference, 1990; Liège, Belgium, 1377-86.

Jain AK, (1989). Fundamentals of digital image processing. Prentice Hall, Englewood Cliffs, 16-18.
Russ JC, Dehoff RT (2000). Practical Stereology. 2nd edition, Plenum Press, New York.

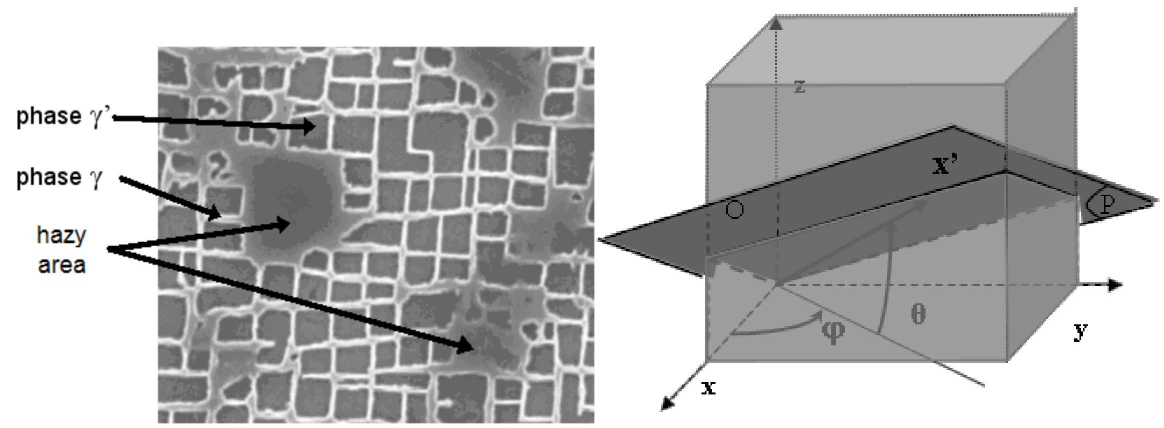

Fig. 1 (a) Section of a nickel base superalloy (b) Section plane azimuth φ and elevation θ

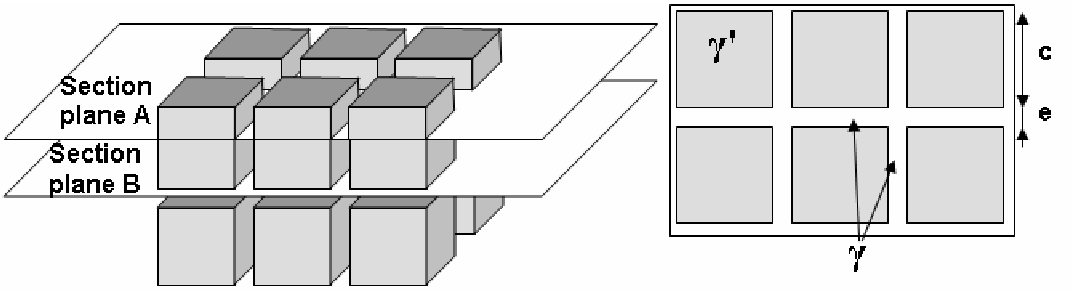

Fig. 2 (a) Cubic grid model with φ=0° and θ=0°. (b) Image of section plane A.

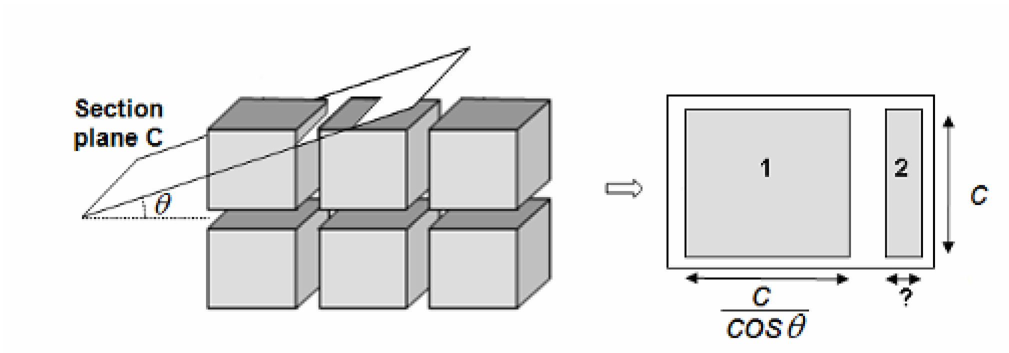

Fig. 3 Cubic grid model for φ=0° and θ≠0° and the related image of the section plane.

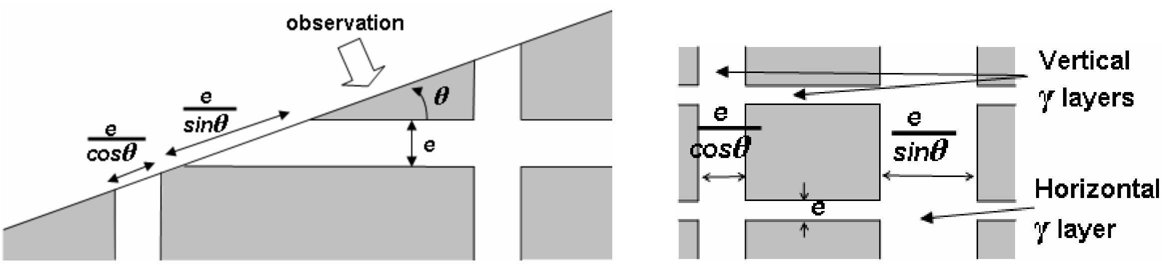

Fig. 4 (a) Vertical view for φ=0° and θ=20° (b) Image of the oblique section plane

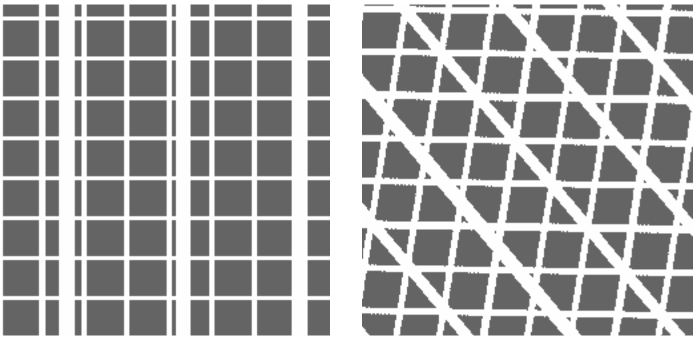

Fig. 5 Section simulations (a) φ=0°, θ=20° (b) φ=45°, θ=20°

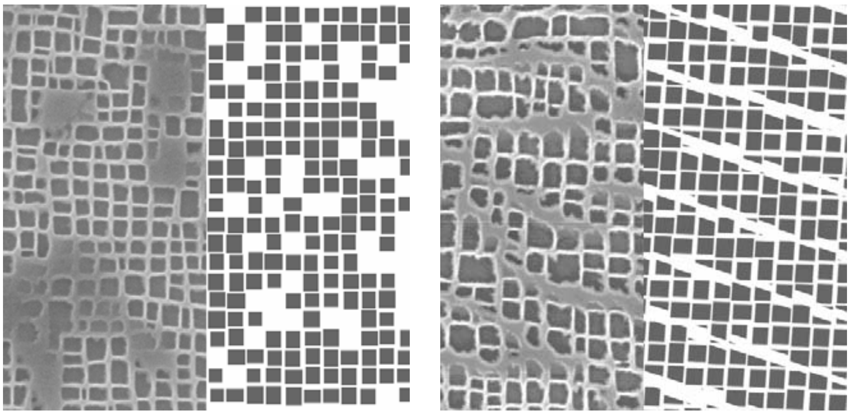

Fig. 6 Real section and simulations using the realistic model (a) φ=0°, θ=0° (b) $\varphi \neq$ 0°, $\theta \neq$ 0°.

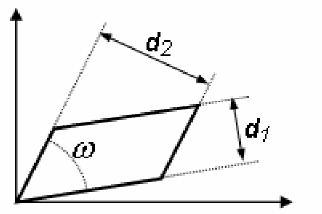

Fig. 7 Parallelogram-shaped γ’ particle

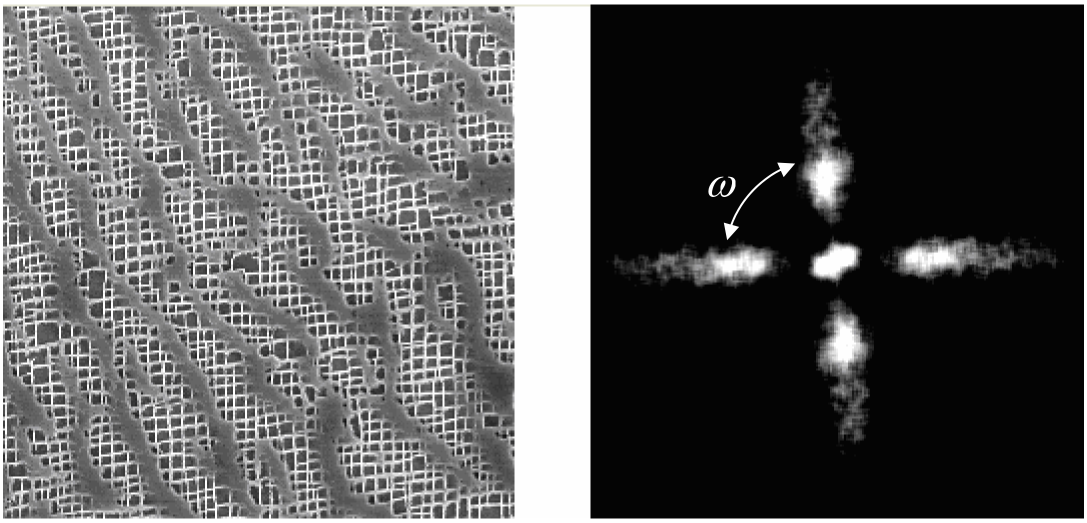

Fig. 8 (a) Real image from an oblique section   (b) Corresponding Fourier Spectrum

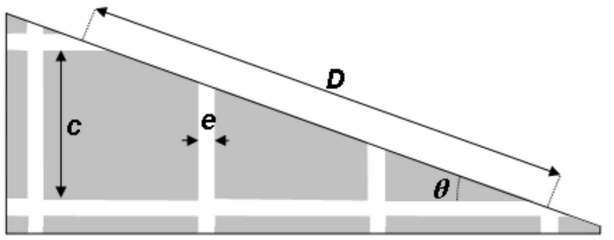

Fig. 9 Distance D between two consecutive hazy areas

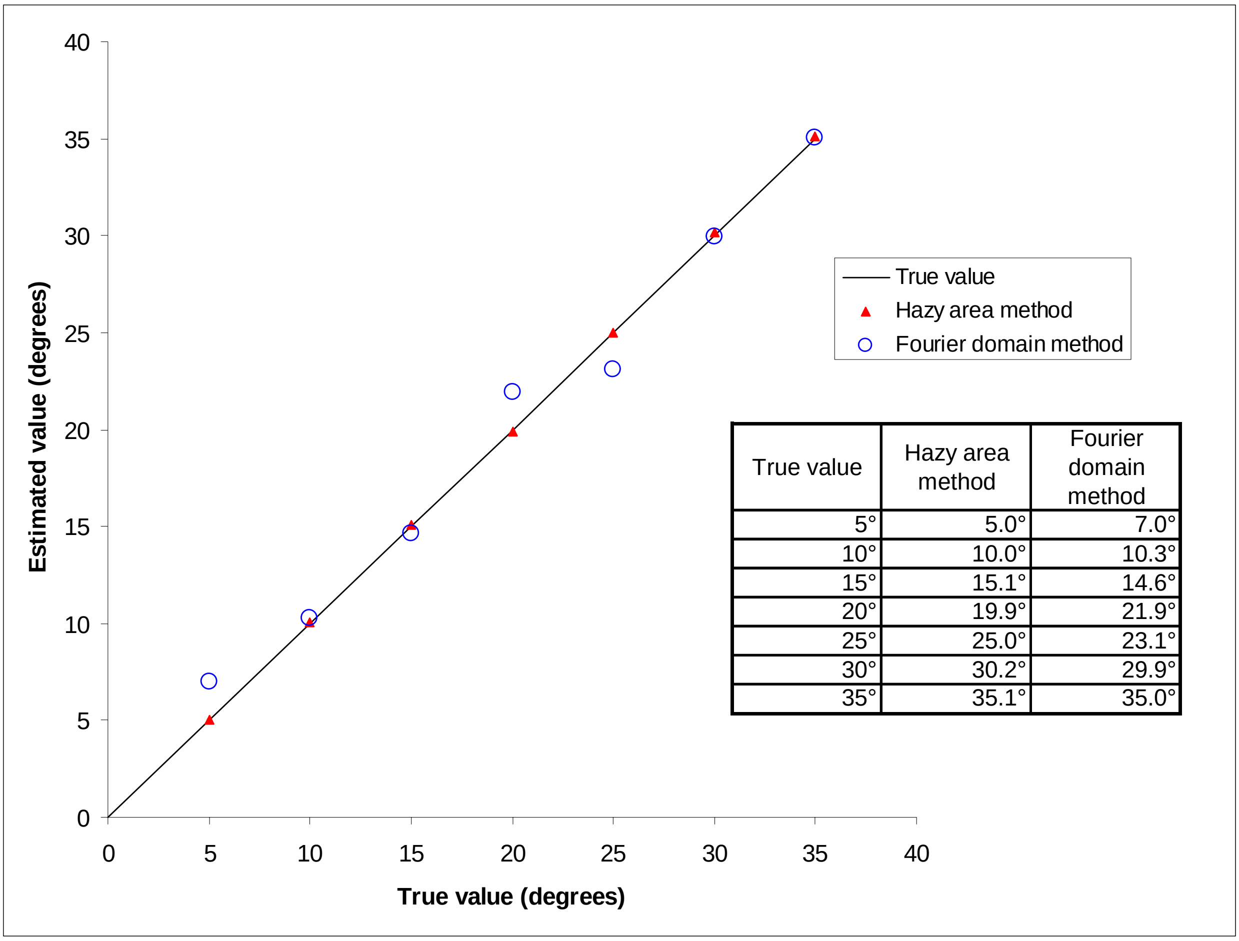

True value	Hazy area method	Fourier domain method
5°	5.0°	7.0°
10°	10.0°	10.3°
15°	15.1°	14.6°
20°	19.9°	21.9°
25°	25.0°	23.1°
30°	30.2°	29.9°
35°	35.1°	35.0°

Fig. 10. Estimation of θ using synthetic image coming from 3D models section

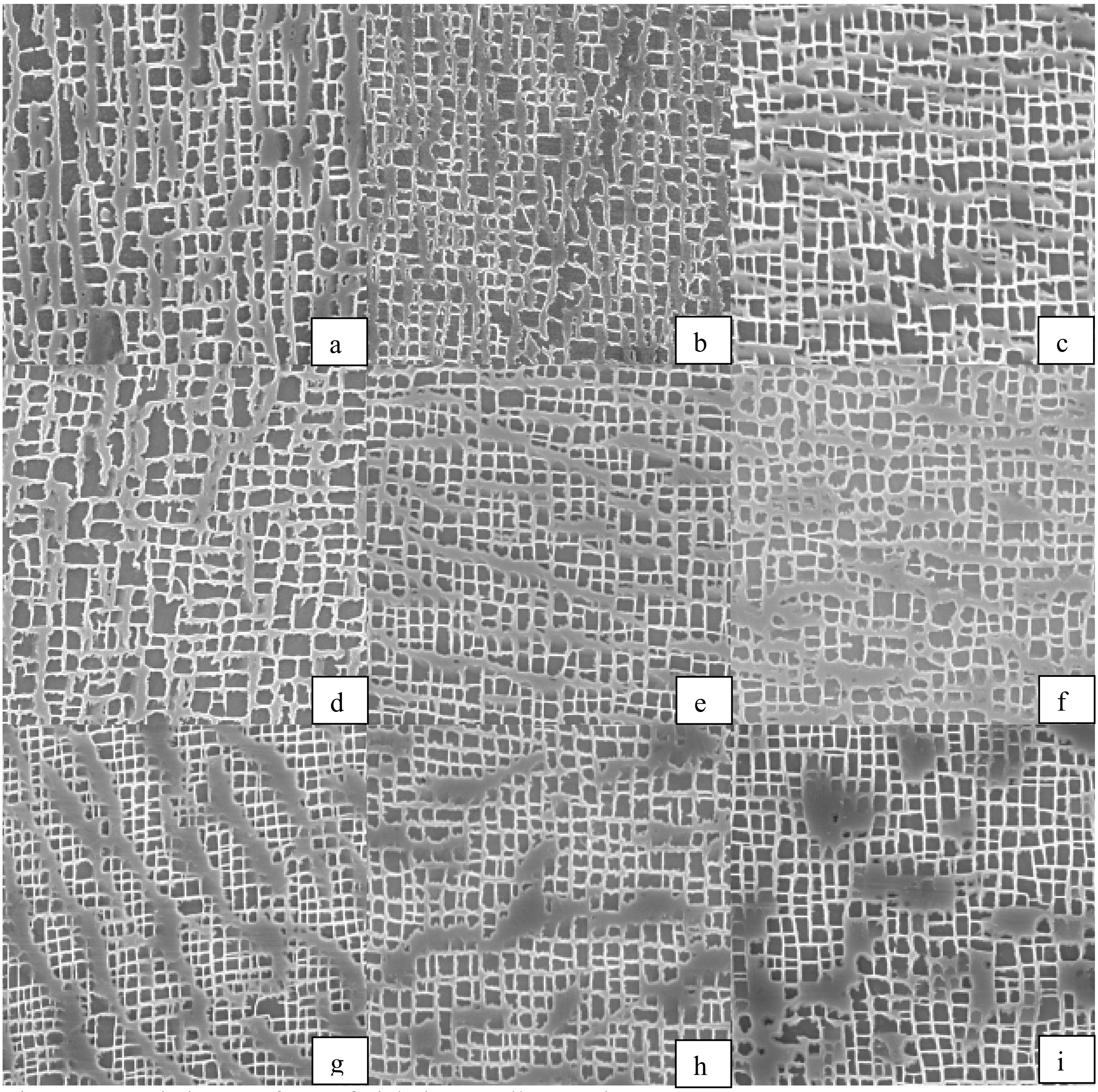

Fig. 11. Sample images from of nickel superalloy sections

Image	Estimation using hazy areas	Estimation using Fourier	Average of both estimations	Variation between both methods
a	37.7°	34.7°	36.2°	3.0°
b	31.0°	31.6°	31.3°	0.6°
c	29.7°	31.7°	30.7°	2.0°
d	22.0°	22.2°	22.1°	0.2°
e	21.1°	18.4°	19.7°	2.7°
f	20.6°	17.3°	18.9°	3.3°
g	14.1°	18.1°	16.1°	4.0°
h	12.6°	16.8°	14.7°	4.2°
i	<5°	<5°	<5°	NC

Table 1: Elevation angle estimations for samples in Fig. 11

Image	Correction factor (Hazy areas)	Correction factor (Fourrier)	Average correction factor	Variation between both methods
a	+11.0%	+9.3%	+10.2%	+1.7%
b	+7.4%	+7.7%	+7.6%	+0.3%
c	+6.8%	+7.8%	+7.3%	+1.0%
d	+3.7%	+3.8%	+3.7%	+0.1%
e	+3.4%	+2.6%	+3.0%	+0.8%
f	+3.2%	+2.3%	+2.8%	+1.0%
g	+1.5%	+2.5%	+2.0%	+1.0%
h	+1.2%	+2.2%	+1.7%	+0.9%
i	0%	0%	0.0%	0.0%

Table 2: Correction factor estimations for samples in Fig. 11